

A review of high frequency surface wave radar for detection and tracking of ships

Anthony M. PONSFORD, Jian WANG

*Raytheon Canada Limited, 400 Phillip Street, Waterloo Ontario,
N2L 6R7, CANADA
e-mail: tony_ponsford@raytheon.com, jian_wang@raytheon.com*

Abstract

In today's resource-driven economy, maritime nations are claiming economic borders that extend beyond the continental shelf or the 200 nautical mile (nm) Exclusive Economic Zone (EEZ). However, claiming such large economic area places responsibilities on the parent nation to exercise jurisdiction through surveillance and enforcement.

The requirement to see beyond the horizon has long been a goal of maritime security forces. Today, this is largely dependent on cooperative vessels voluntarily communicating their intentions to local shore-side authorities, as well as on those vessel sightings reported by patrollers. Recent advances in technology provide maritime nations with options to provide more systematic surveillance of both cooperative and non-cooperative targets.

This paper presents an overview of a land-based High Frequency Surface Wave Radar (HFSWR) used to provide persistent, active, surveillance. The paper demonstrates that these radars have now reached a level of maturity where their performance is predictable and that they can, within known limits, reliably detect and track ocean going vessels throughout the EEZ.

1. Introduction

This paper provides an overview of factors that affect the performance of HFSWR and how these systems can be most effectively used to provide real-time, persistent and active surveillance of the 200 nm EEZ maritime boundaries.

HFSWR refers to a classification of radar that utilizes the surface-wave mode of propagation and that operate in the 3 MHz to 30 MHz frequency range; surface waves have the following characteristics:

- (a) they attenuate directly as functions of distance (range), frequency and surface roughness;
- (b) they propagate efficiently in vertical polarization only; and
- (c) they require a conducting surface, such as a saline ocean, to propagate.

HFSWR detection range is dependent on many factors [1], [2]. For our initial discussion it is sufficient to state that the range obtainable is dependent on the frequency of operation, radiated power and vessel size as

well as the prevailing environmental conditions. The radar signal will experience a greater rate of attenuation as the radar frequency is increased or, for a given frequency, the sea state increases.

Detection of vessels by HFSWR fall in to two distinct categories: those smaller vessels (typically less than 1000 tons) whose detection range is limited by the presence of ocean clutter and those larger vessels (typically greater 1000 tons) whose maximum detection range is limited by external noise. In the former case, the detection range can only be increased by reducing the area of the radar clutter cell, whilst in the latter case the detection range can also be extended by increasing the effective radiated power.

1.1. Paper overview

This paper presents an overview of factors that influence the successful detection and subsequent tracking of vessels using HFSWR. Section 2, introduces the basics of an HFSWR system and presents an example of the layout of a typical radar site. This is followed in Section 3 by a review of propagation losses as a function of both radar frequency and sea state.

The scattering of the radar signal from the ocean and the resulting ocean clutter spectrum is discussed in Section 4. Section 5 reviews vessel detection using HFSWR and presents a method for approximating the radar cross section (RCS) of a vessel at HF. The performance of HFSWR is ultimately limited by external noise and this is discussed in Section 6. The impact on performance of unwanted signals such as self generated ionospheric clutter is presented in Section 7. A key factor in specifying radar performance is the Probability of Detection; this is discussed in Section 8, whilst Section 9 presents an overview of tracking and the associated Probability of Track. Conclusions are presented in Section 10.

2. HFSWR basics

HFSWRs that are used for long-range vessel tracking typically operate in a pulse-Doppler mode, where the radar emits a coherent pulse train. Vessels, which are within the area illuminated by the radar, reflect these pulses back to the radar, where the echoes are received by a linear array of antennas. The signal received on each antenna is digitally processed to enhance the signal-to-interference ratio, where the term interference includes all unwanted signals such as sea clutter, external noise, ionospheric reflection as well as interference from other users of the band. The returned echoes are processed and sorted according to range, velocity (Doppler) and bearing. The echoes are then compared against a detection threshold chosen to achieve a predetermined constant-false-alarm-rate (CFAR). If the magnitude of an echo exceeds the threshold it is declared a detection. These detections are then forwarded to a tracking algorithm that associates consecutive detections in to tracks.

An example of a monostatic radar site is illustrated in Figure 1. It can be observed that in this configuration the transmit and receive arrays are co-located and share a common site. The length of the receive array is a compromise between the desire to maximize the directive gain and resolution whilst minimizing real-estate requirements. This typically limits the number of element pairs to 16 spaced at $1/2\lambda$ increments. Both the transmit antenna and individual doublet-pairs generate antenna patterns that cover the desired search area.

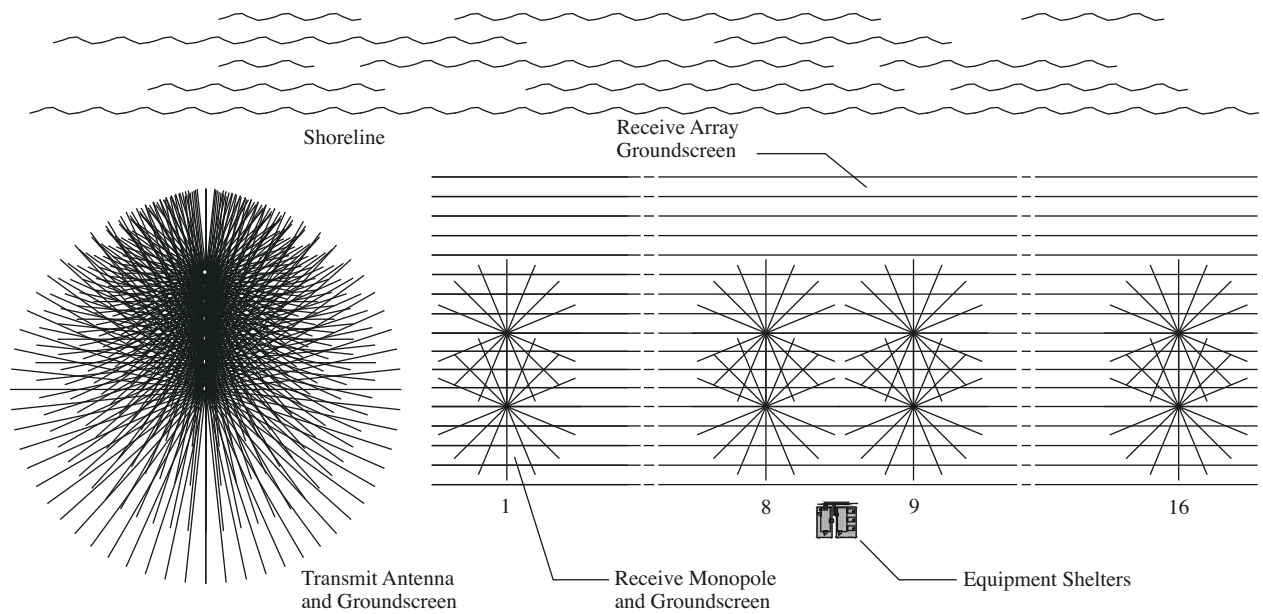


Figure 1. Typical radar site layout for a monostatic installation.

2.1. Radar coverage area

For a monostatic radar, the area of coverage is symmetrical around the radar boresight, where the boresight is perpendicular to the axis of the array. When using a linear array, returns from beyond ± 60 degrees in azimuth are typically not displayed, due to rapid falloff in system performance as well as the potential for left/right ambiguity due to the presence of unwanted grating lobes.

Within the azimuth coverage region, the radar signal processor synthesizes multiple narrow receive beams. These receive beams are “electronically steered” to simultaneously cover the desired search area. As illustrated in Figure 2, as a beam is steered away from boresight it becomes both broader and more lossy.

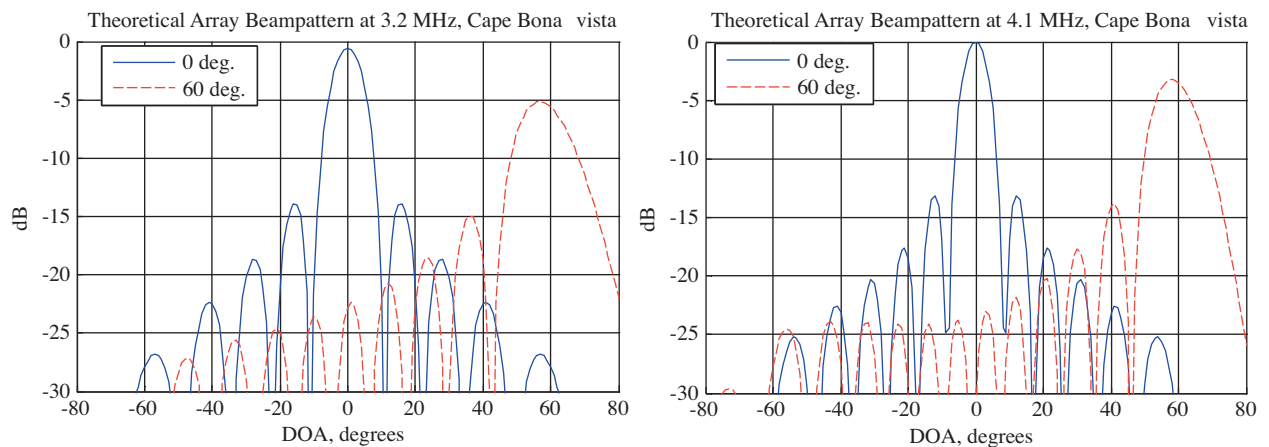


Figure 2. Comparison of receive synthesized beam pattern at boresight and +60 degree for operating frequencies of 3.2 and 4.1 MHz.

When specifying the performance of a HFSWR, it is typical to assume an azimuth-averaged gain of the combined transmit and receive antenna patterns.

3. Propagation losses

HFSWR achieves beyond-the-horizon detection based on surface wave propagation. Surface waves follow the curvature of the earth, since currents are induced at the surface that result in a slowing down of the wave-front close to the ground, causing it to tilt or diffract downwards. This diffraction results in a loss that is proportional to both the conductivity of the surface and wavelength of the radiated signal. For this reason, vessel detection using HFSWR is most effective over saline-ocean and at frequencies below 20 MHz.

Propagation losses derived using the propagation model GRWAVE [3] as a function of frequency, for a smooth ocean, are presented in Figure 3.

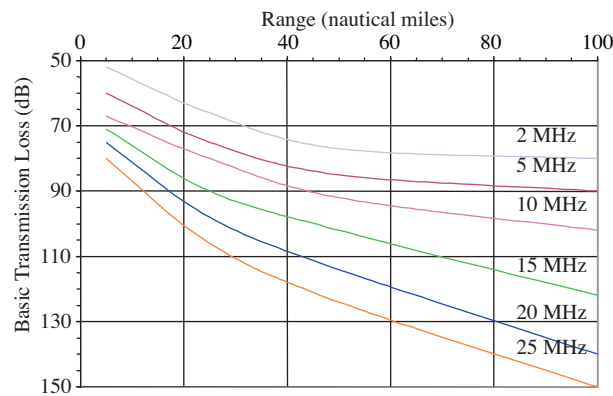


Figure 3. Basic one-way transmission loss as a function of frequency over a standard, smooth, sea. [derived from ITU-R groundwave model (GRWAVE)].

Additional losses also occur with surface roughness [4]. Example plots of the added one-way propagation losses, as a function of wind speed, are presented in Figure 4. In summary, it can be observed that both the propagation losses and added losses due to sea state increase with frequency, as does the rate of increase.

4. Ocean clutter

$f_{ds} = \pm \sqrt{\frac{gf_c}{\pi c}}$ The maximum detection range of smaller vessels is typically limited by the presence of ocean clutter. This ocean clutter spectrum is the result of the interaction of the radiated electromagnetic wave with ocean waves [5], [6], [7]]. For grazing incidence, the dominant interaction, as illustrated in Figure 5a, is the result of first-order scatter from ocean surface waves with a wavelength exactly one-half of the radar carrier wavelength. This results in two large peaks in the sea echo spectrum that are caused by a pairs of ocean waves that are moving directly away from, and directly towards, the radar. The condition is referred to as Bragg resonant scatter. These Bragg lines are symmetrically placed about zero Doppler at Doppler shifts (f_{ds}) that are proportional to the phase velocity of the Bragg-matched ocean waves with wavelengths half that of the

radar carrier frequency (f_c).

$$f_{ds} = \mp \sqrt{\frac{gf_c}{\pi c}} \tag{1}$$

where c is speed of light and g is the acceleration due to gravity.

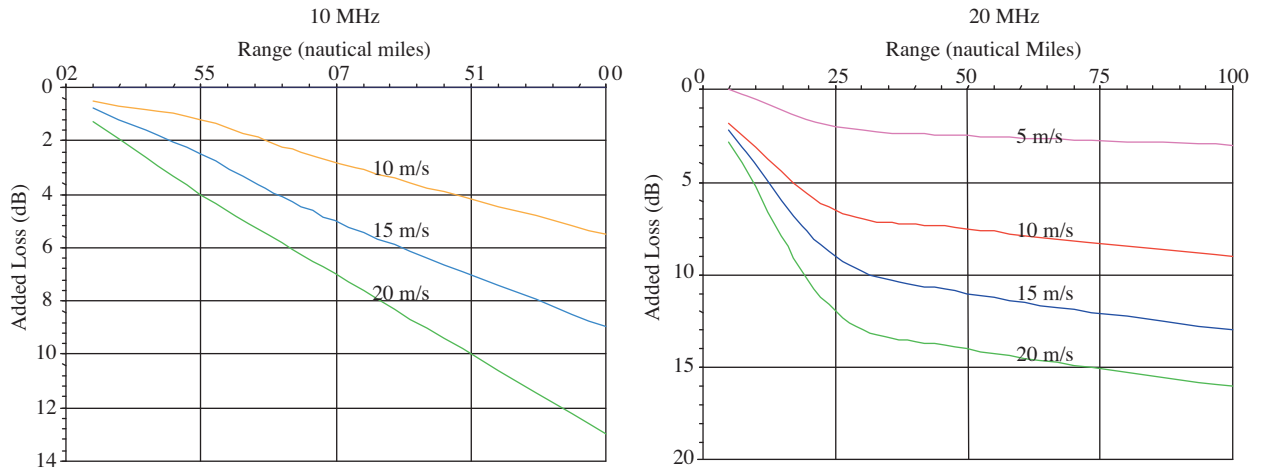


Figure 4. Added loss due to surface roughness (wind speed = 5 m/s, corresponding to sea state 3; 10 m/s, sea state 5; 15 m/s, sea state 7; and 20 m/s, sea state 8).

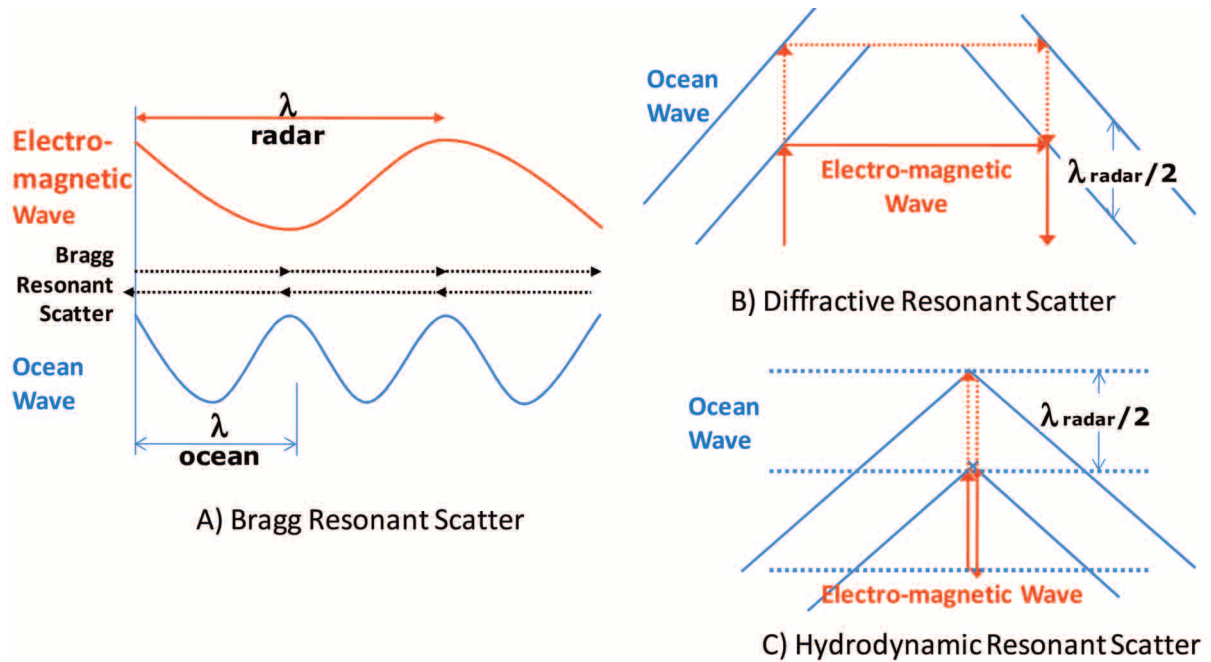


Figure 5. Electromagnetic and ocean wave Interaction that result in both first-order and second-order resonant scatter.

Ocean waves are trochoidal and contain multiple frequencies, and thus Bragg resonant scatter will also occur at harmonics of the principal wavelength. This results in second-order peaks in the ocean spectrum. Also,

since the ocean surface consists of a random collection of sea waves, and the detailed configuration of the ocean surface varies in an irregular manner, additional scattering occurs that results in a continuum.

4.1. Ocean clutter continuum

The ocean clutter continuum is the result of second-order scatter. As illustrated in Figure 5b, if the effective spacing of ocean waves (as seen by the radar) is equal to one-half the radar wavelength, then diffractive scattering will occur along the surface of the specular reflection angle. If these scattered radar waves encounter a second sea wave of suitable wavelength and direction, then the radar signal will be returned to the radar.

A second source of second-order scatter, illustrated in Figure 5c, is the result of interaction between crossing sea waves. If these crossing sea waves generate a third sea wave having a wavelength equal to one-half the radar wavelength, then Bragg resonance scatter will occur.

A modeled power spectrum [8] showing the relative contribution of first- and second-order ocean scattering as observed by an HF Radar is presented in Figure 6. In the figure, the clutter power spectrum has been plotted relative to the equivalent radial speed of a vessel, and where by convention a positive velocity is associated with a vessel approaching the radar. As illustrated in Figure 7, the energy contained within the second-order continuum is related to sea-state and hence surface wind speed.

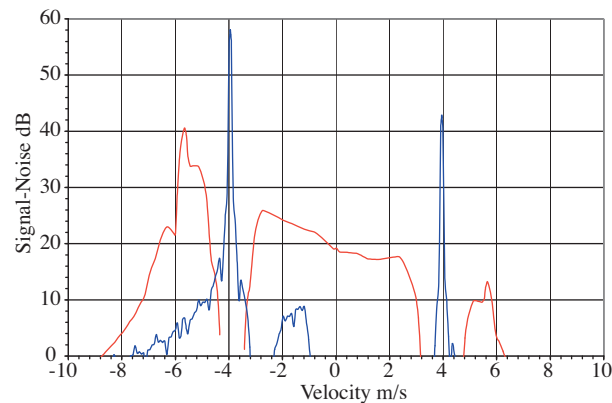


Figure 6. Relative contribution of first (blue trace) and second (red trace) order clutter to the HF radar doppler spectrum radar simulation of a radar operating at 15 MHz at 100 km range, sea-state 8.

In addition, since the wind has a cardioid distribution pattern, the distribution of the energy contained within the second-order continuum will be dependent on the wind direction. For example, Figure 8 compares the theoretical clutter spectrum for winds blowing at $+35^\circ$ and -35° degrees relative to the radar look direction. It can be observed that the spectra are mirror images about zero. For the $+35^\circ$ case, the clutter spectrum has the majority of the energy contained in the negative half of the spectrum, whilst for the -35° wind-direction it is in the positive half. Hence, in the former case, the maximum range at which a small outbound vessel will be detected will be less than for the same vessel when inbound, the opposite being true for the -35° wind.

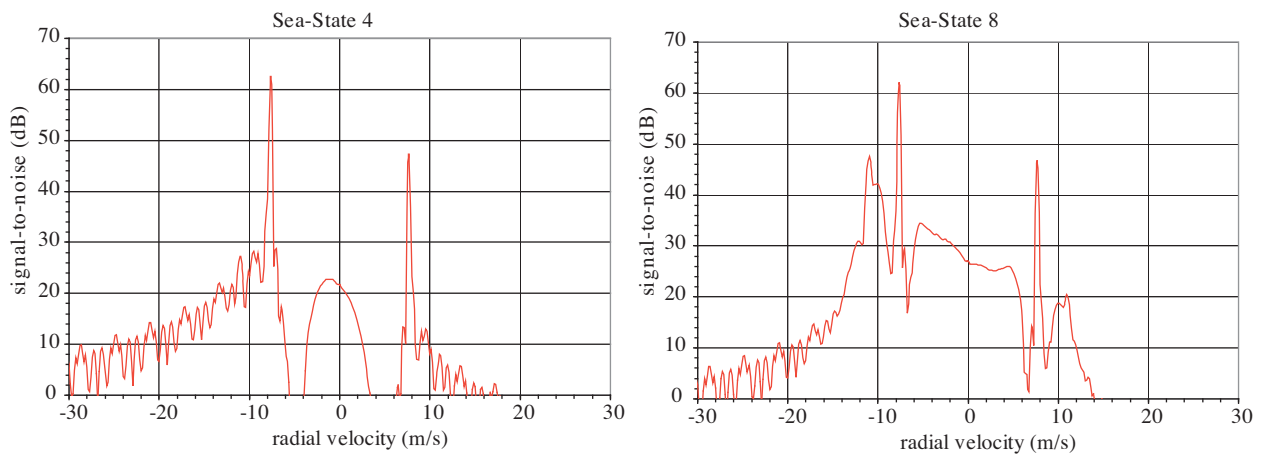


Figure 7. Modelled ocean clutter spectra for sea-state 4 (15 kts wind) and sea-state 8 (35 kts wind), wind direction 60 degrees relative to radar look direction. Radar operating at 3.5 MHz.

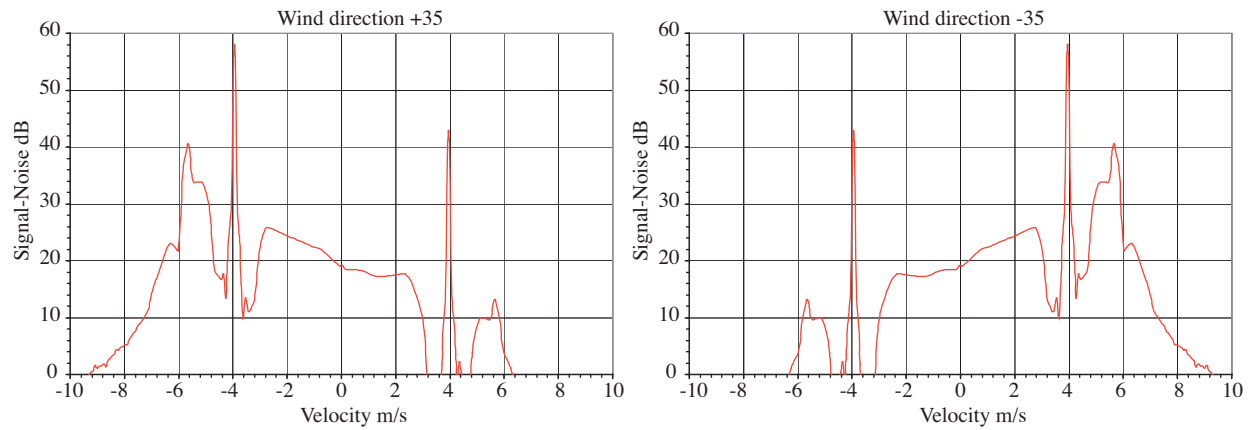


Figure 8. Modelled ocean clutter spectra for 20 knot winds at +35 and -35 degrees, relative to the radar look direction, for a radar operating at 15 MHz.

4.2. Critical frequency

Ocean surface waves are wind-generated. If the sea wave corresponding to the Bragg resonance is fully developed, that is, the energy being added to the waves by the wind is equal to the energy dissipated, the wave spectrum is saturated or in equilibrium. For this to occur, it is required that the following condition has been met:

$$f_{crit} = \frac{cg}{4\pi U^2}. \tag{2}$$

Here f_{crit} is the minimum radar frequency such that the system is in equilibrium and U is the wind speed, c is the velocity of light and g is the acceleration due to gravity.

The spectra presented in this report all assume that the sea state is sufficient such that the radar is operating above the critical frequency. If the radar is operated at a frequency below the critical frequency, the sea will not be fully developed, and the energy contained within the Bragg wave and associated continuum will be significantly less. Under such conditions it is not unusual to detect small vessels to significantly greater ranges.

5. Vessel detection

HFSWRs are coherent devices that discriminate between echoes originating from surface vessels and the usually more dominant sea echo, on the basis of their differing Doppler shifts.

$f_{dt} = \frac{2Vf_c}{c}$ At HF, the dominant return from surface vessels is the result of reflections from vertical superstructure. These echoes will experience a Doppler shift f_{dt} that is proportional to the vessel's radial velocity V with respect to the radar look direction:

$$f_{dt} = \frac{2Vf_c}{c} \quad (3)$$

5.1. Vessel detection within the ocean clutter spectrum

Ocean-clutter usually limits the detection range of small to medium size vessels. For vessel detection, the magnitude of the clutter against which the vessel is detected is determined by the magnitude of the continuum at the radial velocity corresponding to that of the vessel, this being determined by the radar frequency as well as the wind speed and direction relative to the radar. Detection of smaller, low-speed vessels will therefore be heavily influenced by the continuum level and hence wind-speed and wind direction. In the specification of the radar performance, it is typical to assume a Doppler averaged value for the continuum for all wind directions.

Once the sea reaches a fully developed state, an increase in wind speed or surface roughness results in an increase in the extent of the continuum and, since the sea is in equilibrium, does not result in an increase in magnitude. However, for a clutter-limited vessel, there will be a reduction in detection range due to the increase in propagation loss [9]. In addition, at higher frequencies and higher sea states, harmonics associated with Bragg resonant scatter begin to appear.

5.2. Radar blind velocity

It can be observed that returns from the Bragg-matched ocean wave result in a pair of blind velocities equal to the apparent velocity of the Bragg wave. From equation (3) it can be observed that the Doppler shift of an echo originating from a surface vessel is proportional to the radar carrier frequency. However, from equation (1) the Doppler shift of the Bragg-matched wave is proportional to the square-root of the radar carrier frequency. Therefore, as illustrated in Figure 9, to avoid radar blind velocity zones, the radar can be operated simultaneously on two frequencies that are separated according to the formula

$$f_{c2} \geq \left(\sqrt{f_{c1}} + n f_{res} \sqrt{\frac{\pi c}{g}} \right)^2 \quad \text{or} \quad f_{c2} \leq \left(\sqrt{f_{c1}} - n f_{res} \sqrt{\frac{\pi c}{g}} \right)^2 \quad (4)$$

where f_{c1} and f_{c2} are the two carrier frequencies, f_{res} is the Doppler resolution bin, and n is the required number of separation in Doppler from Bragg lines in order for a target to be detected.

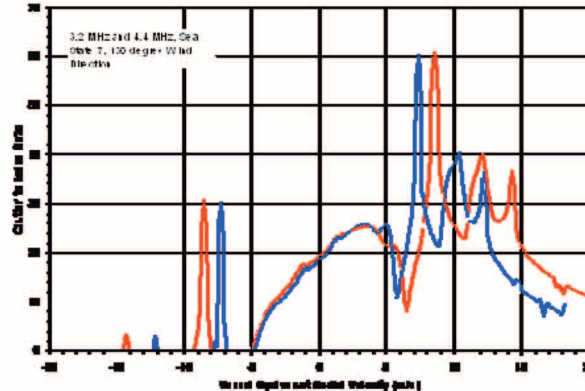


Figure 9. Comparison of the radar ocean clutter spectrum for operation at 3.2 MHz (blue trace) and 4.4 MHz (red trace) in sea-state 7 for a wind direction of 160 degrees relative to the radar look direction.

5.3. Doppler resolution

The Doppler resolution, and hence the radial velocity resolution, is inversely proportional to the coherent integration interval (CII). A sufficient CII must be used to resolve the vessel echo from the more dominant Bragg-matched echo. The CII must also provide enough gain to lift the coherent return from the vessel above that of the non-coherent background noise. In general, it is better to maximize the CII to the limit where the target remains within the given radar resolution cell (range, azimuth, Doppler) and does not suffer either range walk or Doppler smearing.

The limiting factor in setting the duration of the CII is generally determined by the vessel speed and apparent radial acceleration when moving perpendicular to the radar look direction [10]. As illustrated in Figure 10, when the vessel is tangential to the radar look direction, its relative radial velocity and hence Doppler is zero. As the vessel continues on its path it will experience radial acceleration. This radial acceleration will in turn set a limit on the maximum CII if Doppler smearing and corresponding loss of coherent gain is to be avoided.

In summary, the CII is a compromise between various conflicting requirements. It is desirable, in a multi-target environment, to maximize the CII to provide sufficient Doppler resolution as well as provide sufficient processing gain to detect vessels at greater range. However, this has to be traded against the requirement for the vessel response to remain within a radar resolution cell to prevent either range-walk or Doppler smearing. [11]. To overcome these conflicting requirements, the received data can be split and processed, within the signal processing architecture, using multiple CII's.

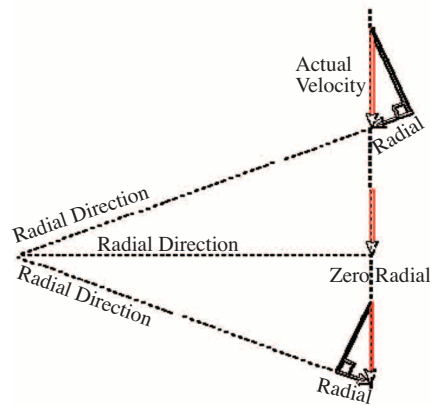


Figure 10. Vessel with a tangential path to the radar look direction.

5.4. Radar cross-section of marine vessels

There are a number of conventions used in defining the radar cross-section (RCS) of a vessel, depending on how the ground plane on which it is situated is treated. This report defines the RCS as if it were measured in free space.

For a vessel to be detected, its radar cross section must be greater than that of the contending RCS of the ocean clutter continuum at the vessel Doppler frequency, The magnitude of the clutter RCS is given by the RCS of the unit patch area multiplied by the area of the radar patch.

The radar cross section of vessels at HF is complex and has been treated extensively by others [12], [13], [14]]. However, it has been shown [15] that the RCS of larger vessels (> 1000 tons) can be approximated by the empirical formula

$$\sigma = 52fD^{3/2} m^2 \quad (5)$$

where σ is the vessel's Free Space RCS, f is the radar frequency in MHz and $D = \text{ship size in } \times 10^3 \text{ metric tons}$.

The RCS of smaller vessels can be approximated as discussed in the following section.

5.5. Radar cross section of small vessels

The RCS of small vessels is dominated by their vertical metallic superstructure. If this superstructure is grounded to the ocean surface, then the RCS of the vessel can be approximated to that of a grounded monopole antenna [16]. When the metallic vertical superstructure is isolated from the ground, then the RCS can be approximated to that of a dipole antenna. Multiple structures will produce additive effects that can result in higher peaks in the RCS value as well as deeper nulls.

Small craft without significant vertical superstructures will have very small RCS, and may only be detected against a noise background. This requires that the boat travels at a radial velocity sufficient such that the resultant Doppler shift is well removed from that of the ocean clutter.

5.5.1. Free space radar cross section of a grounded monopole

$\sigma \approx \frac{(G\lambda)^2}{\pi}$ A monopole antenna cannot be driven in free space; however, the convention of defining antenna gain in free space is convenient and consistent with other antenna definitions, and yields the correct result. The RCS of a resonant monopole in Free Space can be approximated from the equation

$$\sigma \approx \frac{(G\lambda)^2}{\pi} \tag{6}$$

where G is the equivalent Free Space Gain of a Monopole at resonance and is -0.85 dBi.

Deriving the RCS of a non resonant monopole is complex; however, at frequencies below resonance, an f^8 drop-off in RCS can be assumed, and the RCS above resonance can be approximated to that of a resonant monopole antenna at that frequency.

Figure 11 presents a plot of the approximate Free Space RCS of various grounded metallic masts as a function of frequency. The resonance value is derived from Equation 6. The RCS below resonance is derived based on a f^8 roll-off, whilst the dashed curve represents the loci of resonance peaks and can be used to approximate the RCS for frequencies above resonance.

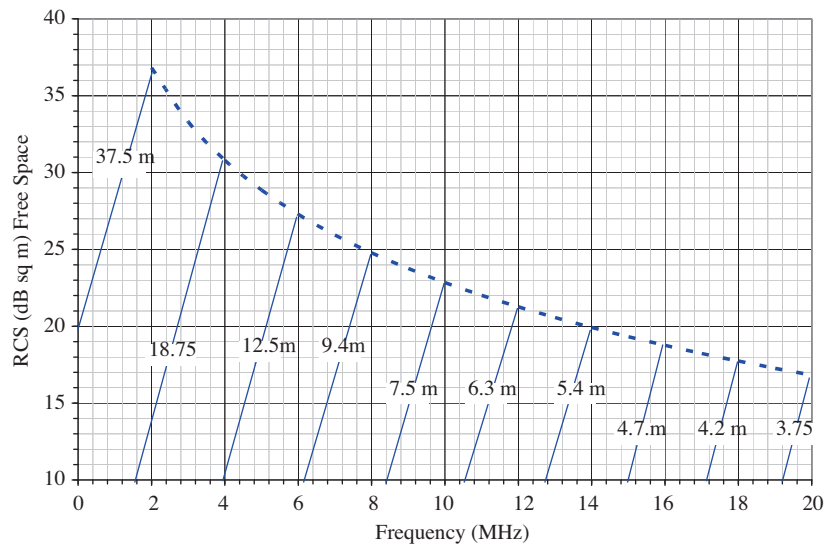


Figure 11. Theoretical RCS of fishing vessels at HF based on the vertical extent of the metallic superstructure.

5.6. Non grounded superstructure

If the metallic superstructure on a vessel is not grounded to the ocean, then it acts as an equivalent vertical dipole in Free Space. The RCS of a resonant dipole is 6 dB greater than that of an equivalent resonant monopole. The RCS below resonance is again derived assuming an f^8 roll-off and the loci of resonance peaks used to approximate the RCS for frequencies above resonance.

Lowering the dipole antenna from free space to the surface of the ground modifies the radiation resistance of the antenna, which is accounted for by the antenna (ground) proximity loss factor. This loss as a function

of height above the ground is plotted in Figure 12. Since the vertical superstructure acts as both receive and transmit antenna, this effect must be entered twice to arrive at the approximation of the RCS. As can be seen, when the dipole is bisected by the ground, it has the same equivalent gain as that of a monopole antenna.

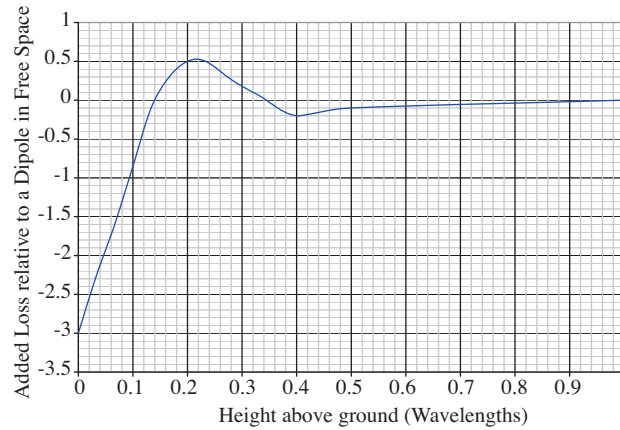


Figure 12. Ground proximity effect showing added loss relative to a dipole antenna in free space as the antenna approaches and eventually dissects the conducting plane.

5.7. Aspect angle dependency

The Radar Cross Section is the sum of reflections of the radar signal from vertical structures. As illustrated in Figure 13, if the apparent distance between these vertical structures as seen by the radar is equal to an even number of quarter wavelengths, then constructive interference takes place. If the apparent distance is equal to an odd number of quarter wavelengths, then destructive interference occurs.

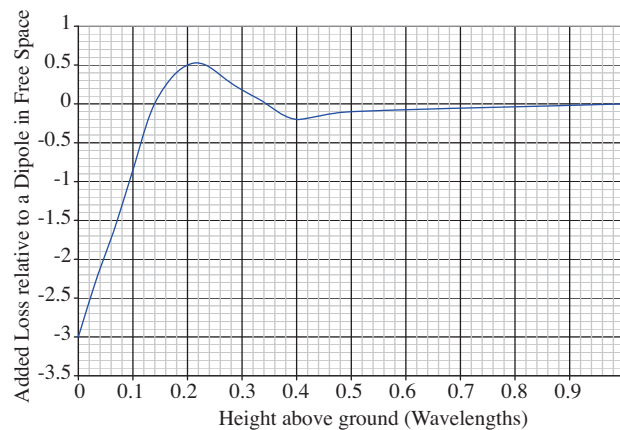


Figure 13. Aspect angle dependence of RCS: constructive and destructive interference.

In summary, HFSWR radiate a vertically polarized wave, and for smaller vessels the RCS is dominated by their vertical superstructure. For larger vessels, the RCS increases with the size of the vessel. Constructive and destructive reflections result in the RCS value changing with the vessel aspect angle relative to the radar

look direction. In general, for larger vessels the broadside RCS is larger than the bow-on or stern-on RCS. In the specification of the RCS of a vessel, it is usual to quote an aspect-angle averaged value for the RCS.

It can be noted that a significant fluctuation in RCS of smaller vessels also occurs as a function of sea state. In higher sea conditions, the pitching and rolling of the vessels reduces the average effective vertical height of the metallic superstructure as observed over the coherent integration interval.

6. External noise

The level of the external noise ultimately limits the maximum detection range of larger vessels. External noise consists of both the irreducible natural noise and the incidental man-made noise. The natural noise is the sum of the atmospheric noise (which is frequency-, location-, season- and time-of-day dependent) and galactic noise (which is frequency-dependent). The level of the man-made noise is determined by frequency and proximity to local noise-generating sources such as industry, power lines and highways. Typical relationships between the various noise sources, as a function of frequency, for a European location are presented in Figure 14.

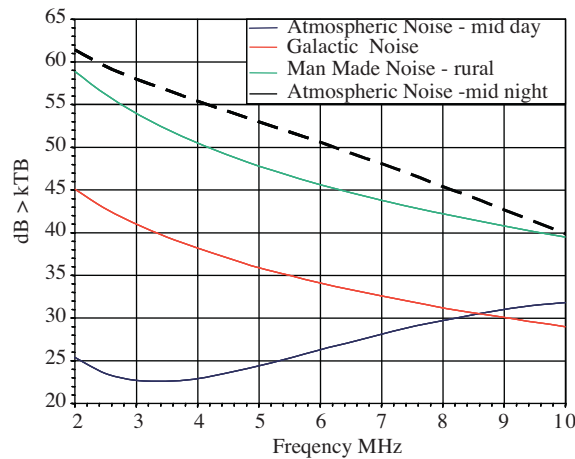


Figure 14. Relationship between the various noise sources as a function of frequency at a European location.

It can be observed that the man-made noise level will typically dominate the day-time noise level; however, at night the atmospheric noise level will usually dominate. Both atmospheric and man-made noise decrease as a function of frequencies; above approximately 15 MHz there is little day/night dependency. It can also be observed that at frequencies below 10 MHz the contribution of galactic noise can be ignored.

6.1. Man-made noise

The daytime noise level at a site will typically be dominated by man-made noise. Man-made noise is dependent on the level of human activity, and can be approximated by [17] the relation

$$N_m = c - d \log 10f - 20dBW, \quad (7)$$

where N_m denotes man-made noise power in decibels below 1 W in a 1 Hz bandwidth, f is frequency in MHz, and c, d are constants derived from measurements.

Constants c and d have been derived by the Comité Consultatif International des Radio Communications (CCIR) as shown in Table 1.

Table 1. Constants c and d derived by the Comité Consultatif International des Radio Communications (CCIR).

Environmental Category	c	d
Business Stores, offices, industrial parks, etc	76.8	27.7
Residential > 5 dwellings / Hectare	72.5	27.7
Rural < 0.5 dwellings / Hectare	67.2	27.7
Quiet rural	53.6	28.6

It is preferable to select an HF Radar site where the level of man-made noise is low, and it is general to initially specify HFSWR performance relative to that of a typical rural site occurring in the summer month.

Figure 15 presents the predicted atmospheric noise level at 3.5 MHz for a location in Europe. It can be observed that the night time atmospheric noise is considerably greater than the day time atmospheric noise (in this example ~ 10 dB), where the increase is due to impulsive noise arising as the result of lightening, and is greatest at the equator and minimal at the poles. It can also be noted that there is also a fluctuation in noise between the seasons, with the lower noise levels occurring in the summer month.

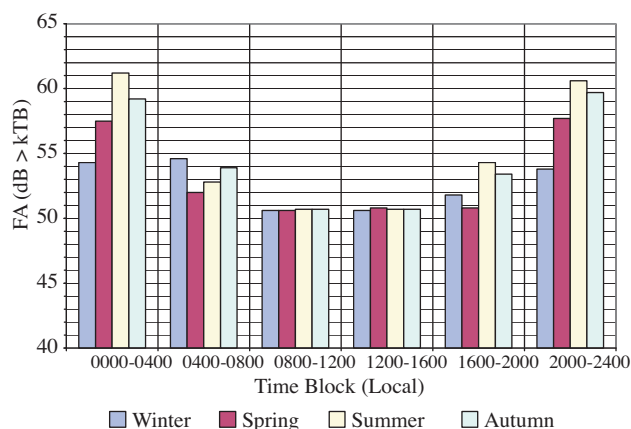


Figure 15. Example estimate of the atmospheric noise level at 3.5 MHz for a location in Europe as a function of time, day and season.

In summary, the background noise level ultimately limits the detection range of larger vessels. In the specification of radar performance, it is usual to present detection range for both day and night using noise values that are averaged over the seasons and time blocks.

7. Ionospheric clutter

Not all the energy emitted by the HF radar propagates along the surface as a surface wave. Some of this energy is directed upwards and may reflect from the ionosphere [1, [18]]. During daylight hours the absorptive properties of the D-layer prevents significant energy being returned to the earth. However, at night this layer disappears and energy is returned via the F-layer.

There are three main categories of ionospheric clutter: a single-reflection or first-order scatter that is the result of a single overhead reflection; second-order scatter, where the signal is initially reflected from the ionosphere, back to the ocean, and forward as a surface wave back to the radar (or vice versa); and third-order scatter, where the signal is reflected via the ionosphere onto the ocean, and from the ocean back to the ionosphere, and subsequently back to the radar.

Typically, due to the geometry of the third-order scatter, the total path length places this clutter beyond the maximum range of the radar, and appears as range-wrap, where the radar receives returns from previous pulses while collecting data on the current transmit pulse. This type of clutter can be readily removed by changing the phase codes of successive pulses of the coherent pulse chain; the second-time-around echo will be heavily attenuated by the filter that is matched to the current pulse, and not the previous.

For second-order ionospheric clutter to be of concern, the total path length must be less than the maximum range of the radar. This limits the reflective angle to near-vertical incidence. For strong reflections to occur from the ocean, it is required that the condition of Bragg resonant scatter is met. At near-vertical illumination this requires ocean waves that have a wavelength that is now equal to that of the radar wavelength. At the lower end of the HF band this implies very high sea states. Strong second-order ionospheric clutter is generally observed in the radar data during periods of high sea-states. It occurs at a range that is equal to the height of the ionospheric F-layer, and extends out in range whilst maintaining approximately the same signal strength.

First-order ionospheric scatter appears at a narrow band of ranges corresponding to the height of either the E- or F-layers. Options for combating this clutter are limited, but it can be alleviated by using multiple radar frequencies that may be returned from slightly different heights [19]. Other options include increasing the radar carrier frequency to above the layer-critical frequency, such that the radar signal penetrates the layer instead of reflecting from it. This typically requires operating at a frequency above 10 MHz. However, the additional surface wave propagation loss may result in the maximum detection range of the radar to be less than the range at which ionospheric clutter occurs.

8. Probability of detection

The previous sections have described the basic radar performance as well as the signal environment. For the data to be useful, it is necessary that the returns from the vessels must be extracted from this environment with a high degree of probability. This is achieved by comparing each radar pixel that is bounded in Azimuth, Range and Doppler, to that of its neighbour. A typical HFSWR may have in the order of 10 million pixels per CII. An efficient detector for determining the presence of a vessel return is the Constant False Alarm Rate (CFAR) algorithm, where a threshold is set such that the rate at which the false alarm occurs due to noise crossing the threshold (in the absence of signal) is constant.

A basic CFAR algorithm is illustrated in Figure 16. The pixel under test is centred in the middle of the range/Doppler/azimuth space. A guard window is employed to ensure that the target is not present in the region used to estimate the noise floor.

In specifying the performance of the radar, it is required that the probability of falsely declaring the presence of a vessel is specified, as well as the probability of correctly declaring the presence of a vessel. This is usually achieved based on theoretical analysis, and requires that appropriate models are used to characterise both the vessel and the environment.

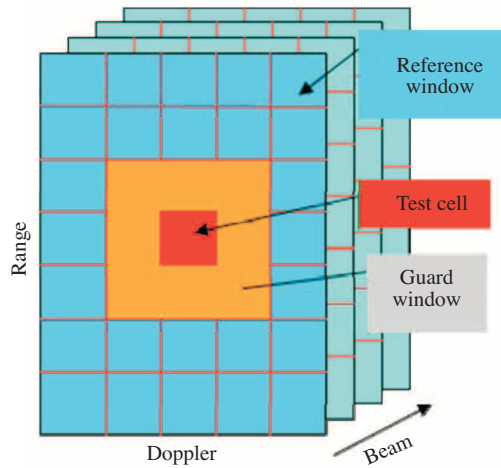


Figure 16. CA-CFAR reference window and guard window.

In the analysis that follows, a Swerling Case-1 model has been used to represent the fluctuations of a vessel, with the results compared to a non-fluctuating scenario. The vessel detection is assumed to be noise-limited, where the noise is Gaussian distributed with zero mean. When a square-law detector is applied, both targets and noise are exponentially distributed. The probability of false alarm P_{fa} is given by the relation

$$P_{fa} = \exp \left[-\frac{T}{\sigma_n^2} \right], \quad (8)$$

where T is the detection threshold and σ_n^2 is the *mean* noise power.

The probability of detection is

$$P_d = \exp \left[-\frac{T}{1 + SNR} \right], \quad (9)$$

where σ_T^2 is the average signal power and $SNR = \sigma_T^2/\sigma_n^2$ is the signal to noise ratio.

Figure 17 presents the probabilities of detection as a function of signal-to-noise ratio. The dotted and solid traces are associated with non-fluctuating and Swerling 1 targets, respectively.

8.1. Tracking and probability of track

For the radar data to be useful, vessels must be displayed on a screen as tracks. A Tracker forms a track by associating consecutive detections that lie within the neighbourhood of the predicted future position of the previous detection or track. The neighbourhood is determined by the expected dynamics of the target motion that places constraints in Range, Azimuth, Doppler and Power.

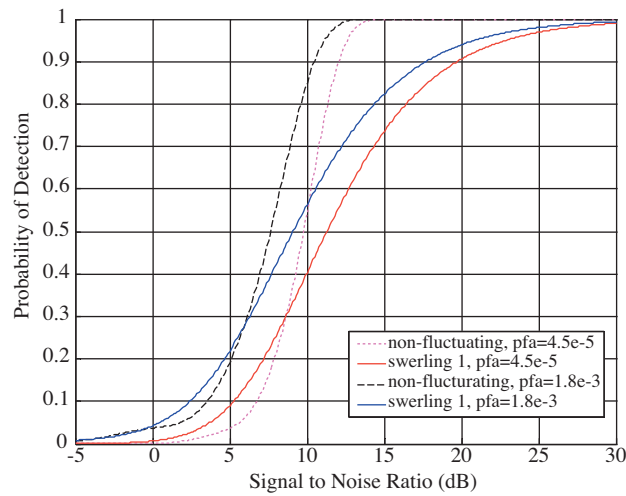


Figure 17. The probability of detection as a function of signal-to-noise ratio.

When a vessel is detected for the first time, a track initiation process is commenced, as illustrated in Figure 18.

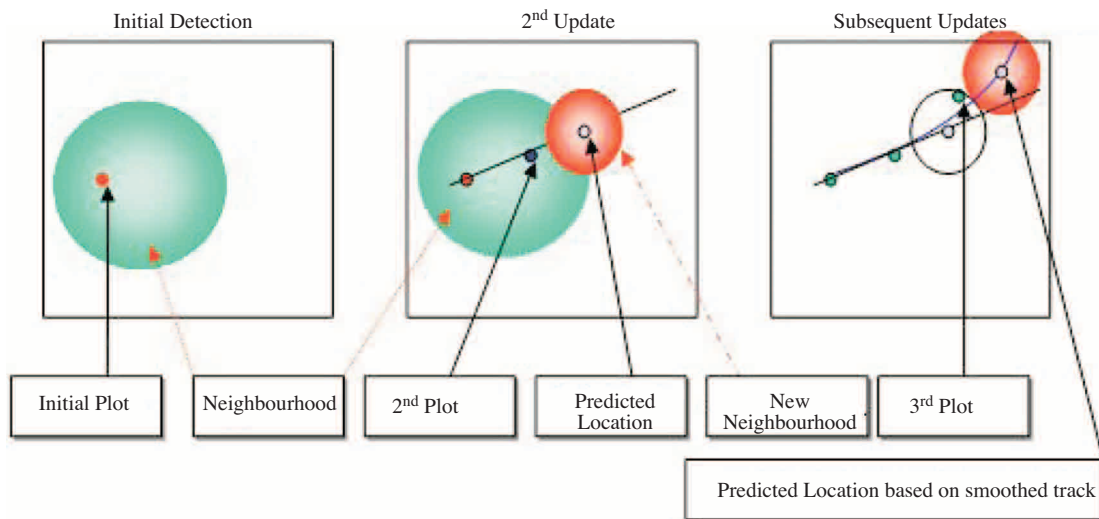


Figure 18. Track initiation process.

Based on the radar parameters, and the limits set on the vessel dynamics, a neighbourhood is drawn around the initial plot or detection. The neighbourhood is not centred on the plot, since the plot also has a Doppler associated with it. For example, if this Doppler is significantly positive, then the vessel is approaching the radar. Therefore, it is reasonable to predict that the next return from this vessel will be at a range that is closer to the radar by an amount that is related to the measured Doppler. Since the radar only measures the radial component, the vessel may be travelling to the left or right of the radar; consequently, the direction of travel can not be determined until at least two updates have been received. The Tracker outputs a “smoothed” target location based on the weighted average of the predicted and measured locations.

To minimize false track rates, a deferred decision Tracker can be used, where the tracker employs three levels of track promotion logic:

1. Potential tracks (P): single detection
2. Tentative tracks (T): 0-X update tracks
3. Confirmed tracks (C): track is deleted after a defined number of consecutive misses.

The probability of track is defined as the likelihood that a vessel detected with a given Probability of Detection (P_d) forms a confirmed track. The probability of confirmed track is dependent on the Probability of Detection and the Track Promotion Logic, as illustrated in Figure 19.

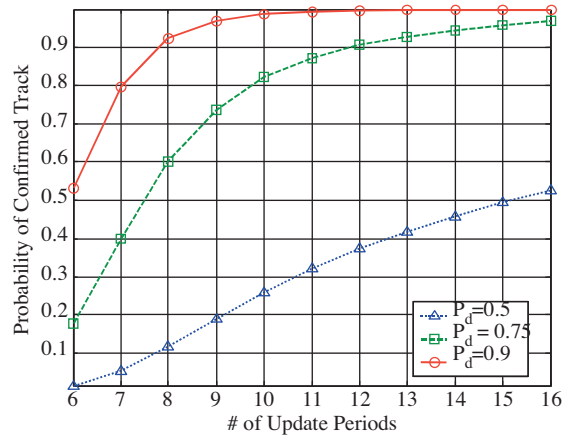


Figure 19. Probability of track as a function of number of updates and probability of detection for logic 2-5-7 (2 associated detections for tentative, 5 associated detections for confirmed and 7 misses to delete).

The probability of detection will generally improve as a vessel approaches the radar, as the propagation path decreases and the signal power increases. Therefore, it is likely that a track will be initiated quicker than that indicated in Figure 19. The minimum number of associated detections required to confirm a track is normally limited by the requirement to maintain a low probability of false track. In general, the fewer the number of associated detections required to confirm a track, the higher the false track rate.

9. Conclusion

This paper has presented an overview of the factors that influence the performance of an HFSWR system. It has been shown that these radars, when operated at the lower end of the HF band, can be used to reliably detect and track ocean going vessels throughout the 200 nm EEZ.

It has been shown that the characteristics and dynamics of a vessel, as well as the background clutter and noise environment, play a significant role in determining radar performance.

It has also been shown that, in general, the variability in detection range can be minimised by operating the radar simultaneously on two frequencies, and by using multiple Coherent Integration Intervals optimised for both radial- and tangential-moving vessels.

Acknowledgements

The authors would like to acknowledge and thank Defence Research and Development Canada (DRDC), for their consistent support in the development and testing of High Frequency Surface Wave Radar.

References

- [1] L. Sevgi, A. Ponsford, A. Chan, "An integrated maritime surveillance system based on high frequency surface wave radars, Part 1 - Theory of operation", IEEE Proc. Ant. And Prop., Vol. 43, Aug. 2001.
- [2] A. Ponsford, L. Sevgi, A. Chan, "An integrated maritime surveillance system based on high frequency surface wave radars, Part 2 - Operational status and system performance", IEEE Proc. Ant. And Prop., Vol. 43, Oct 2001.
- [3] GRWAVE available from <http://www.itu.int/ITU-R/study-groups/software/rsg3-grwave.zip>.
- [4] D. E. Barrick, "Theory of HF and VHF propagation across the rough sea", Parts 1 and 3, Radio Science., Vol. 6, no. 5, pp 517-533, 1971.
- [5] D. E. Barrick, "Remote sensing of sea state by radar", Remote Sensing of Troposphere, V.E. Derr, Ed., GPO, Washington, DC, Ch.12 1972.
- [6] E. D. R. Shearman, "Propagation and scattering in MF/HF ground wave radar", Proc. IEE, Part F, Vol. 130, no. 7, pp 579-590, 1983.
- [7] S. K. Srivastava, "Scattering of high frequency electromagnetic waves from an ocean surface: An alternative approach incorporating a dipole source", Ph.D. Thesis, Memorial University, Newfoundland, 1984.
- [8] D. S. Bryant, A. M. Ponsford, S. K. Srivastava, "A computer package for the parameter optimization of ground wave radar", Proc. OCEANS'88 Conference, USA, Vol. 2, pp 485-490, 1988.
- [9] H. Leong, A. Ponsford, "The effects of sea clutter on the performance of HF surface wave radar in ship detection", IEEE Radar Conference, Italy 2008.
- [10] R. M. Dizaji, A. Ponsford, "Optimum coherent integration time for a surface target with periodic acceleration", IEEE CCECE 2003, Montreal, May 2003.
- [11] A. M. Ponsford, "Detection and tracking of go-fast boats using HFSWR", SPIE Defence and Security Symposium, Orlando ,17 April 2004.
- [12] L. Sevgi, "Target reflectivity and RCS interactions in integrated maritime surveillance systems based on surface wave high frequency radars", IEEE Ant and Prop Mag, Vol. 43, No 1, Feb 2001.
- [13] C. W. Trueman, S. J. Kubina, "RCS of fundamental scatterers in the HF band", 7th Annual Review of Progress in Applied Computational Electromagnetics of the Applied Electromagnetics Computational Society, Monterey, California, March 18-22, 1991.
- [14] H. Leong, H. Wilson, "An estimation and verification of vessel radar cross sections for HFSWR", IEEE Ant and Prop Mag, Vol. 48, no. 2, pp. 11-6, Apr. 2006.

- [15] A. M. Ponsford, "Surveillance of the 200 nautical mile exclusive economic zone (EEZ) using high frequency surface wave radar (HFSWR)", Canadian Journal of Remote Sensing, Vol. 27, No. 4, Aug. 2001, Special Issue on Ship Detection in Coastal Waters, pp. 354-360.
- [16] R. W. Bogle, D. B. Trizna, "Small boat HF radar cross sections", NRL Memorandum Report 3322, July 1976.
- [17] CCIR, "Man-made radio noise", Report 258-4, CCIR, ITU, Geneva, 1986.
- [18] A. Ponsford, R. M. Dizaji, R. McKerracher, "HF surface wave radar operation in adverse conditions", IEEE Proc. Of the Int. Conf. On Radar, Adelaide, Australia, 3-5 Sept. 2003
- [19] H. Leong, A. Ponsford, "The advantage of dual-frequency operation in ship tracking by HF surface wave radar", International Radar Conference 2004, Toulouse, France, 19-21 Oct. 2004.